DØ Note 6177-CONF

Search for the Standard Model Higgs Boson in $\gamma\gamma + X$ final states at DØ using 8.2 fb^{-1} data

The DØ Collaboration
URL http://www-d0.fnal.gov
(Dated: April 28, 2011)

This note describes a search for a light Higgs boson in the di-photon final state using 8.2 fb^{-1} of the DØ Run II data, collected at the Fermilab Tevatron collider from April 2002 to December 2010. Good agreement between the data and the Standard Model (SM) background prediction is observed. We set 95% C.L. upper limits on the production cross section times the branching ratio ($\sigma \times BR(H \rightarrow \gamma\gamma)$) relative to the SM Higgs prediction for different assumed Higgs masses. The observed limits ($\sigma(limit)/\sigma(SM)$) range from 9.5 to 22 for Higgs masses from 100 to 150 GeV, while the expected limits range from 10.5 to 19.

Preliminary Results for Winter 2011 Conferences

I. INTRODUCTION

In the Standard Model (SM), the Higgs boson (H) is the last undiscovered particle that provides crucial insights on the spontaneous breaking of electroweak symmetry and mass generation of electroweak gauge bosons and fermions. The combination of constraints from direct searches at LEP [1] and from precision electroweak observables result [2] in a preferred range for the Higgs boson mass of $114.4 < M_H < 185$ GeV at 95% C.L. The region of $158 < M_H < 175$ is excluded by a combination of searches at CDF and DØ [3–6]. In this note, we report on a search for the SM Higgs boson in an inclusive event sample containing two photons. The search for this particular decay mode is challenging because of the small di-photon branching ratio of the SM Higgs; for instance it is about 0.22% for $M_H = 130$ GeV. On the other hand, the two-photon signature is clean and sensitive to all three production mechanisms (gluon-gluon fusion, associated production, weak-boson fusion), and leads to an experimental search which can constrain models beyond the SM in which this branching ratio can be significantly enhanced [7].

The previous analysis [8] used 4.2 fb^{-1} of DØ Run II data to search for high mass $\gamma\gamma$ resonances by examining the invariant mass of the di-photon system $M_{\gamma\gamma}$. In this note, we use 8.2 fb^{-1} of DØ Run II data and adopt a Multivariate Analysis Technique (MVA) [9], which brings an improvement of the sensitivity relative to that merely using $M_{\gamma\gamma}$.

II. DØ DETECTOR AND DATA SAMPLE

The DØ detector is comprised of a central tracking system in a 2 T superconducting solenoidal magnet, a liquid-argon/uranium calorimeter, a preshower detector and a muon spectrometer [10]. The major parts of the DØ detector used in the event selection are the tracking system, the electromagnetic (EM) calorimeter and the central preshower detector (CPS). The tracking system consists of a silicon microstrip tracker (SMT) and an eight-layer scintillating fiber tracker (CFT). The calorimeter has a central section (CC) covering up to $|\eta_{det}| \approx 1.1$ [11], and two end components (EC) extending coverage to $|\eta_{det}| \approx 4.2$. Each section is housed in a separate cryostat, and divided into EM layers on the inside and hadronic layers on the outside. The EM calorimeter has four longitudinal layers and transverse segmentation of 0.1×0.1 in $\eta_{det} - \phi_{det}$ [11] space except in the third layer (EM3), where it is 0.05×0.05. Immediately before the inner layer of the central EM calorimeter, there is CPS formed of two radiation length of absorber followed by three layers of scintillating strips with embedded wavelength-shifting fibers. Luminosity is measured using plastic scintillator arrays located in front of the EC cryostats. The data acquisition system consists of a three-level trigger, designed to accommodate the high instantaneous luminosity. For final states containing two photon candidates with transverse energy above 25 GeV, the trigger efficiency is close to 100%. The data sample used in this analysis was collected between April 2002 and December 2010 and corresponds to an integrated luminosity of 8.2 ± 0.5 fb^{-1} after applying standard data quality requirements.

The SM Higgs Monte Carlo (MC) samples, are generated using PYTHIA [12] with CTEQ6L [13] parton distribution functions (PDFs), and processed through a GEANT-3 based [14] simulation of the DØ detector. In order to accurately model the effects of multiple $p\bar{p}$ interactions and detector noise, data events from random $p\bar{p}$ crossings with a similar instantaneous luminosity spectrum as considered in the data analysis are overlaid on the MC events. These MC events are then processed using the same reconstruction software as the data. Samples corresponding to each of the three dominant SM Higgs boson production mechanisms are normalized using the next-to-next-to-leading order (NNLO) theoretical cross sections for gluon fusion and vector boson associated production, and NLO for vector boson fusion production [15]. The branching ratio predictions are from HDECAY [16]. The gluon fusion production cross section is also corrected for two-loop electroweak effects [17].

III. EVENT SELECTION

Events are selected requiring at least two photon candidates with $E_T > 25$ GeV and $|\eta_{det}| < 1.1$. Photons are selected from EM clusters reconstructed within a cone of radius $\mathcal{R} = \sqrt{(\Delta\eta)^2 + (\Delta\phi)^2} = 0.2$ and satisfying the following requirements: (i) At least 95% of the cluster energy is deposited in the EM calorimeter; (ii) The calorimeter isolation variable $I = [E_{\rm tot}(0.4) - E_{\rm EM}(0.2)]/E_{\rm EM}(0.2)$ is less than 0.1, where $E_{\rm tot}(0.4)$ is the total energy in a cone of radius $\mathcal{R} = 0.4$ and $E_{\rm EM}(0.2)$ is the EM energy in a cone of radius $\mathcal{R} = 0.2$; (iii) The energy-weighted cluster width in EM3 is consistent with an EM shower; (iv) The scalar sum of the transverse momentum p_T of all tracks originating from the primary vertex in an annulus of $0.05 < \mathcal{R} < 0.4$ around the cluster ($\sum p_T^{\rm trk}$) is less than 2 GeV; (v) In order to suppress electrons misidentified as photons, the EM clusters are required to not be spatially matched to tracker activity (track veto), i.e. either to a reconstructed track, or to a set of hits in the SMT and CFT consistent with that of an electron trajectory; (vi) The contribution of jets misidentified as photons is reduced by combining the information from a set of variables sensitive to differences between photons and jets in the tracker activity and

in the energy distributions in the calorimeter and CPS, using an artificial neural network (ANN) [18]. The variables used are: $\sum p_T^{\rm trk}$, the number of cells above a certain threshold requirement in the first EM calorimeter layer within $\mathcal{R} < 0.2$ and $0.2 < \mathcal{R} < 0.4$ of the EM cluster, the number of associated CPS clusters within $\mathcal{R} < 0.1$ of the EM cluster, and a measure of the energy deposition width in the CPS. The ANN is trained using di-photon and di-jet MC samples and its performance is verified using a data sample of $Z \to \ell^+\ell^-\gamma$ ($\ell = e, \mu$) events [8]. Fig. 1 compares the ANN output (O_{NN}) distribution for photons and jets. Photon candidates are required to have an ANN output O_{NN} larger than 0.1. Such a requirement is almost 100% efficient for photons while rejecting $\sim 40\%$ of misidentified jets. (vii) Additionally, the di-photon invariant mass is required to be larger than 60 GeV, and the azimuthal angle between the two photon candidates is required to be larger than 0.5.

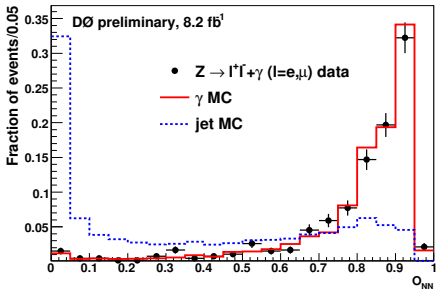

FIG. 1: Normalized distributions of O_{NN} value from real and fake photons.

IV. BACKGROUNDS

There are three major sources of background to the $H \to \gamma\gamma$ signature: (i) Drell-Yan events, where both electrons are misidentified as photons; (ii) γ+jet and jet+jet events where the jet(s) are misidentified as photon(s); (iii) direct di-photon events. The modeling of individual backgrounds is described in the following sections.

A. Drell-Yan $Z/\gamma^* \to ee$ contribution

We use $Z/\gamma^* \to ee$ PYTHIA MC samples to estimate the Drell-Yan contribution. The NNLO cross section [19] is used for the normalization. From the $Z/\gamma^* \to ee$ MC samples, we find that 2% of the electrons can pass the photon selection requirements described in Section III due to tracker inefficiencies. The total background contribution from the Drell-Yan process is found to be 699 ± 15 events.

B. γ+jet and di-jet background

We estimate the γ + jet and di-jet contributions from the data with the final event selection applied (see section III) by using the method described in detail in Ref. [20]. In this analysis, we use $O_{NN} = 0.75$ as a boundary to classify the candidates into four categories:

- N_{pp} have both photon candidates with $O_{NN} > 0.75$;
- N_{pf} have the leading photon candidate with $O_{NN} > 0.75$, but the sub-leading $O_{NN} < 0.75$;
- N_{fp} have the leading photon candidate with $O_{NN} < 0.75$, but the sub-leading $O_{NN} > 0.75$;
- N_{ff} have both photon candidates with $O_{NN} < 0.75$.

The Drell-Yan Z/$\gamma^* \to ee$ contributions to (N_{pp}, N_{pf}, N_{fp}, N_{ff}) are determined from MC simulation and are subtracted. The pass-fail vector (N_{pp}, N_{pf}, N_{fp}, N_{ff}) thus obtained is related to the ($N_{\gamma\gamma}, N_{\gamma j}, N_{j\gamma}, N_{jj}$) vector as follows:

$$\begin{pmatrix} N_{ff} \\ N_{fp} \\ N_{pf} \\ N_{pp} \end{pmatrix} = E \times \begin{pmatrix} N_{jj} \\ N_{j\gamma} \\ N_{\gamma j} \\ N_{\gamma\gamma} \end{pmatrix} \tag{1}$$

where the $N_{\gamma\gamma}$ is the number of γ+γ events, $N_{\gamma j}$ and $N_{j\gamma}$ are the number of γ+jet events and N_{jj} is the number of di-jet events. The 4×4 matrix E is defined as:

$$\begin{pmatrix} (1-\epsilon_{j1})(1-\epsilon_{j2}) & (1-\epsilon_{j1})(1-\epsilon_{\gamma 2}) & (1-\epsilon_{\gamma 1})(1-\epsilon_{j2}) & (1-\epsilon_{\gamma 1})(1-\epsilon_{\gamma 2}) \\ (1-\epsilon_{j1})\epsilon_{j2} & (1-\epsilon_{j1})\epsilon_{\gamma 2} & (1-\epsilon_{\gamma 1})\epsilon_{j2} & (1-\epsilon_{\gamma 1})\epsilon_{\gamma 2} \\ \epsilon_{j1}(1-\epsilon_{j2}) & \epsilon_{j1}(1-\epsilon_{\gamma 2}) & \epsilon_{\gamma 1}(1-\epsilon_{j2}) & \epsilon_{\gamma 1}(1-\epsilon_{\gamma 2}) \\ \epsilon_{j1}\epsilon_{j2} & \epsilon_{j1}\epsilon_{\gamma 2} & \epsilon_{\gamma 1}\epsilon_{j2} & \epsilon_{\gamma 1}\epsilon_{\gamma 2} \end{pmatrix} \tag{2}$$

where $\epsilon_{\gamma 1}$ and $\epsilon_{\gamma 2}$ are the fractions of the leading and sub-leading photons that have passed the event selection and have $O_{NN} > 0.75$, and ϵ_{j1} and ϵ_{j2} are the fractions of jets that have passed the event selection and have $O_{NN} > 0.75$. The photon efficiency (ϵ_γ) is estimated using direct di-photon MC and corrected for small differences between data and the simulation measured in pure samples of photon events from radiative Z decays $Z \to \ell^+\ell^-\gamma$ ($\ell = e, \mu$). The jet efficiency (ϵ_j) is estimated using di-jet MC enriched in jets misidentified as photons, and cross-checked in jet samples in data. Both efficiencies are parameterized as a function of photon pseudorapidity. ($N_{\gamma\gamma}, N_{\gamma j}, N_{j\gamma}, N_{jj}$) can be obtained by solving the linear equation. Table I shows the results after applying the method to the data.

N_{DY}	699 ± 15
$N_{\gamma\gamma}$	10905 ± 234
$N_{\gamma j} + N_{j\gamma}$	6207 ± 343
N_{jj}	2923 ± 183
Data	20734

TABLE I: The number of $\gamma\gamma$, γ+jet and di-jet events in the data from the 4x4 matrix method. The number of DY events is estimated from MC. The quoted uncertainties are statistical only.

Due to the limited statistics of non-$\gamma\gamma$ (sum of γ+jet and di-jet) events from the 4×4 matrix method, especially in the high mass region, we reverse the event selection cut $O_{NN} > 0.1$ on one or both of the two photon candidates to obtain an enriched γ+jet or di-jet orthogonal sample from data. We find that the kinematic distributions from such "reversed-O_{NN}" samples are in good agreement with the non-$\gamma\gamma$ events from the 4×4 matrix method. Therefore we use the "reversed-O_{NN}" samples normalized by the corresponding numbers of non-$\gamma\gamma$ events from the 4x4 matrix method to model the non-$\gamma\gamma$ background.

C. Direct di-photon production

We use the SHERPA [21] Monte Carlo to model the direct $\gamma\gamma$ background shape and use the di-photon component of the 4x4 matrix method for the normalization. The inclusive cross section of SHERPA has leading order accuracy while the photon fragmentation function is modeled by an interleaved QCD+QED parton shower including higher-order real-emission matrix elements.

V. SYSTEMATIC UNCERTAINTIES

Systematic uncertainties affecting the normalization and shape of the MVA output are estimated for both signal and backgrounds.

- 6.1% uncertainty on the integrated luminosity [22] affecting signal and Drell-Yan background normalization;
- 3% uncertainty on the photon identification efficiency affecting signal and Drell-Yan background normalization;
- 0.7-1.0% uncertainty on the signal acceptance from the PDFs uncertainty, estimated using the CTEQ6M [23] error functions;
- 0.1-1.7% and 1-5% uncertainties on the signal acceptance and shape from gluon fusion signal p_T reweighting to SHERPA.

- 9% uncertainty on the track veto efficiency and 4% on the cross section affecting the Drell-Yan background normalization;
- 3% uncertainty on the photon $O_{NN} > 0.75$ efficiency in the 4×4 matrix method affecting non-$\gamma\gamma$ and $\gamma\gamma$ backgrounds normalization and shape;
- 10% uncertainty on the jet $O_{NN} > 0.75$ efficiency in the 4×4 matrix method affecting non-$\gamma\gamma$ and $\gamma\gamma$ backgrounds normalization and shape.
- 10-20% uncertainty from the factorization and renomalization scale of SHERPA affecting $\gamma\gamma$ background shape.

VI. FINAL DISCRIMINANT DISTRIBUTIONS AND LIMITS

A. Final discriminant distributions

In this analysis, to improve the overall sensitivity, we use the Gradient Boosted Decision Tree method from the Toolkit for Multivariate Analysis [9] that combines five kinematic variables to build a final discriminant between the signal and background. The five kinematic variables we used are,

- leading photon transverse energy, E_T^1;
- sub-leading photon transverse energy, E_T^2;
- di-photon invariant mass, $M_{\gamma\gamma}$;
- di-photon transverse momentum, $p_T^{\gamma\gamma}$;
- azimuthal angle between the two photon candidates, $\Delta\phi_{\gamma\gamma}$.

Fig. 2 shows these five kinematic distributions from data, backgrounds and the $M_H = 125$ GeV signal. The data and background modeling agrees well. The signal and total background samples are trained for every mass point displayed in Table III using events within the [M_H - 30GeV, M_H + 30GeV] mass window. At the 2.5 GeV mass points, we have interpolated the MVA input distributions from the neighbouring 5 GeV points using the fact that the selection efficiency is almost independent of the di-photon mass and the mass resolution is approximately constant ($\sim$ 3 GeV). As an illustration, we show the MVA output distributions for six of the assumed Higgs masses in Fig. 3. Table II shows the signal, backgrounds and data yields for six of the assumed Higgs masses within the $\pm$30 GeV mass window.

	100 GeV	110 GeV	120 GeV	130 GeV	140 GeV	150 GeV
$Z/\gamma^* \to ee$:	629 $\pm$ 14	541 $\pm$ 13	376 $\pm$ 11	140 $\pm$ 7	66 $\pm$ 5	34 $\pm$ 4
Non-$\gamma\gamma$:	5477 $\pm$ 179	3456 $\pm$ 144	2216 $\pm$ 115	1452 $\pm$ 95	967 $\pm$ 80	670 $\pm$ 68
direct $\gamma\gamma$:	6616 $\pm$ 180	4371 $\pm$ 145	2808 $\pm$ 116	1914 $\pm$ 97	1354 $\pm$ 82	998 $\pm$ 69
total background:	12722 $\pm$ 254	8368 $\pm$ 205	5400 $\pm$ 164	3506 $\pm$ 136	2387 $\pm$ 115	1702 $\pm$ 97
Data:	12746	8380	5406	3500	2383	1696
Signal:	5.43 $\pm$ 0.02	5.42 $\pm$ 0.02	5.05 $\pm$ 0.02	4.18 $\pm$ 0.02	3.01 $\pm$ 0.01	1.80 $\pm$ 0.01

TABLE II: Signal, backgrounds and data yields from 100 GeV to 150 GeV in 10 GeV intervals within [M_H - 30GeV, M_H + 30GeV] mass window. The quoted uncertainties are statistical only.

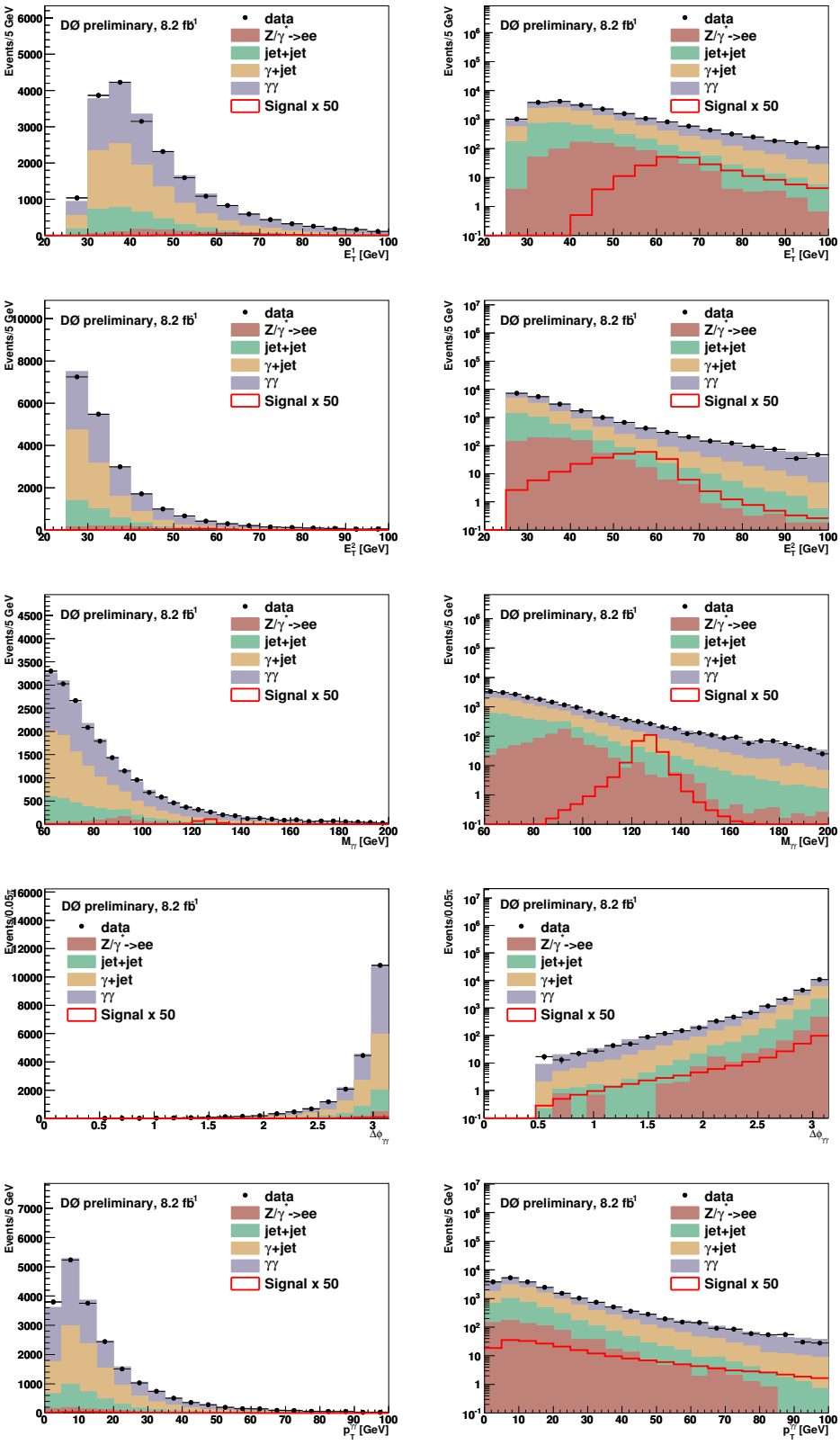

FIG. 2: Data and background modeling comparisons in terms of E_T^1, E_T^2, $M_{\gamma\gamma}$, $\Delta\phi^{\gamma\gamma}$ and $p_T^{\gamma\gamma}$ for the mass region [60, 200] GeV. A signal for $M_H = 125$ GeV is also shown. The plots in the left column are in linear scale and the plots in the right column are in log scale.

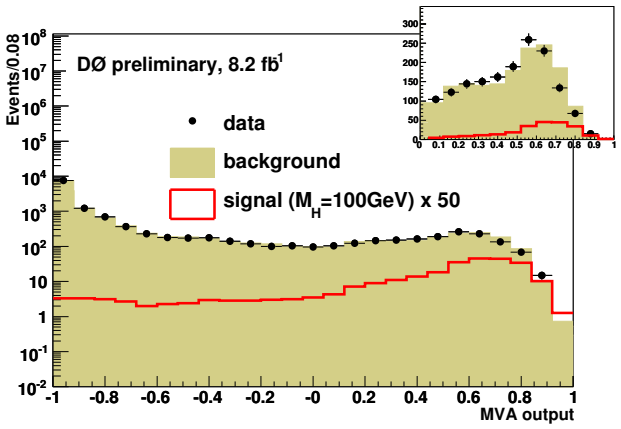

(a) $M_H = 100$ GeV

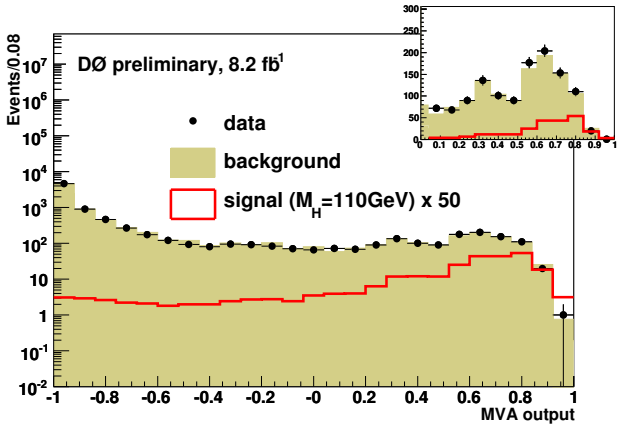

(b) $M_H = 110$ GeV

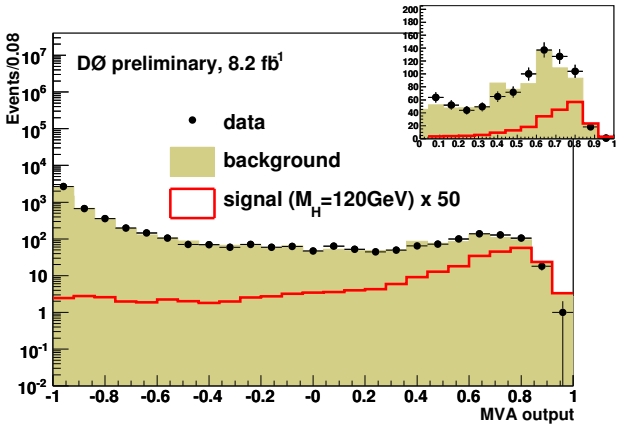

(c) $M_H = 120$ GeV

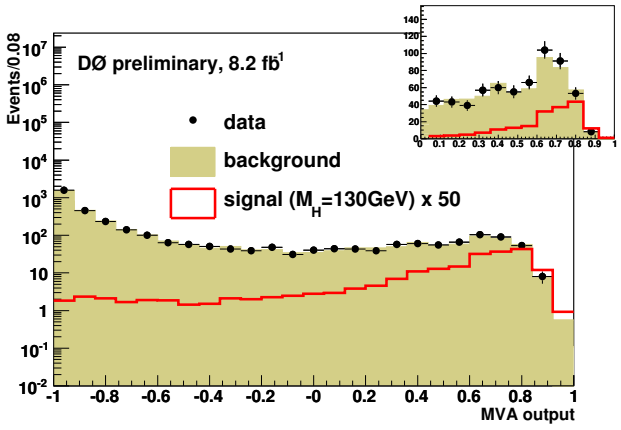

(d) $M_H = 130$ GeV

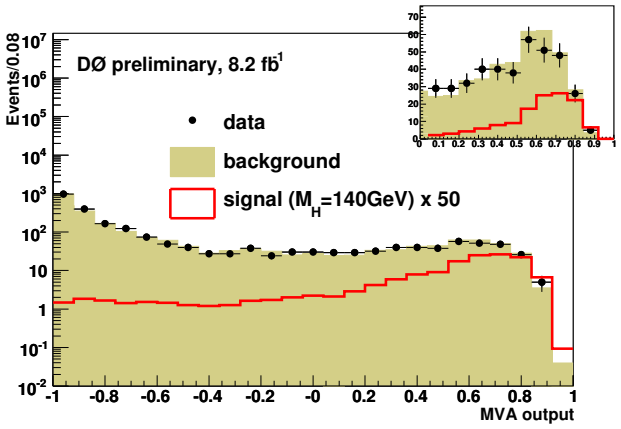

(e) $M_H = 140$ GeV

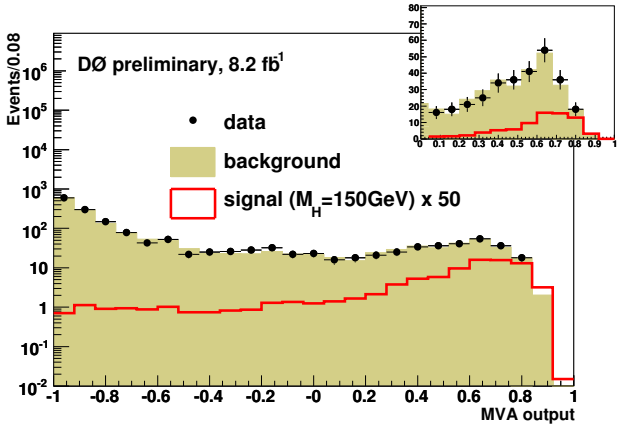

(f) $M_H = 150$ GeV

FIG. 3: MVA output distributions for $M_H = 100 - 150$ GeV in 10 GeV intervals within [M_H - 30GeV, M_H + 30GeV] mass window. The inset figures show the MVA output distributions for the signal concentrated region [0, 1] in a linear scale.

B. Limit setting

Since there is no evidence for new physics, we set upper limits on the Higgs production cross section times branching ratio for Higgs decaying into a pair of photons, using the MVA output distributions for each mass point in the interval of [$M_{\rm H}$ - 30 GeV, $M_{\rm H}$ + 30 GeV]. Limits are calculated at the 95% C.L. using the modified frequentist CL$_s$ approach with a Poisson log-likelihood ratio test statistic [24, 25]. We treat systematic uncertainties as "nuisance parameters" constrained by their priors, and the best fits of these parameters to data are determined at each value of M_H by maximizing the likelihood ratio [25]. The correlations of the systematic uncertainties are maintained.

As an illustration, the background subtracted data distribution is shown in Fig. 4.

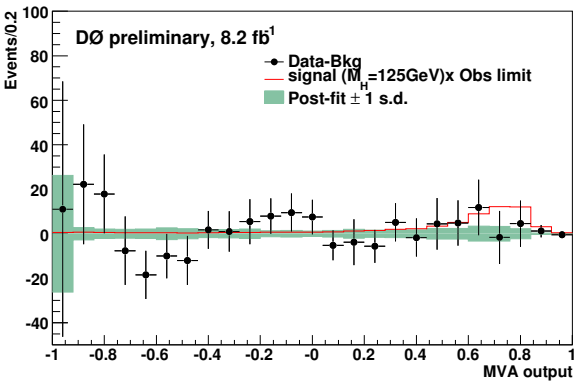

FIG. 4: Post-fit background subtracted data distribution for $M_H = 125$ GeV. The signal is scaled by the observed limit. The green area shows the post-fit 1 standard deviation (s.d.) under the background-only hypothesis.

The resulting 95% C.L. upper limits on the cross section times branching ratio relative to the SM prediction are given in Table III and displayed in Fig. 5 as a function of Higgs boson mass.

Higgs mass(GeV)	100	102.5	105	107.5	110	112.5	115	117.5	120	122.5
observed limit	9.5	10.7	18.1	22.4	19.6	20.3	19.9	14.1	12.4	13.7
expected limit	15.0	14.3	13.4	12.5	11.7	11.3	11.0	10.5	11.3	10.6
SM $\sigma \times BR$(fb)	3.5	3.5	3.4	3.4	3.3	3.3	3.2	3.1	3.0	2.9

Higgs mass(GeV)	125	127.5	130	132.5	135	137.5	140	142.5	145	147.5	150
observed limit	12.9	13.8	15.6	14.9	17.4	13.3	10.6	11.3	12.1	13.8	19.3
expected limit	10.7	10.8	11.0	11.3	11.6	12.5	13.1	14.1	15.3	16.8	18.6
SM $\sigma \times BR$(fb)	2.7	2.6	2.4	2.3	2.1	1.9	1.7	1.5	1.3	1.2	1.0

TABLE III: 95% C.L. limits on $\sigma \times BR$ relative to the SM prediction for different Higgs masses.

VII. SUMMARY

We have presented a search for the SM Higgs boson in the di-photon channel using 8.2 fb^{-1} of DØ Run II data. Good agreement between the data and the SM background prediction is observed. Since there is no evidence for new physics, we set 95% C.L. limits on the production cross section times the branching ratio ($\sigma \times BR(H \to \gamma\gamma)$) relative to the SM Higgs prediction for different assumed Higgs masses. The observed limits ($\sigma(limit)/\sigma(SM)$) range from 9.5 to 22 for Higgs masses from 100 to 150 GeV, while the expected limits range from 10.5 to 19. By comparison with the 4.2 fb^{-1} result [8], the expected limits are improved typically by $\sim$ 70%, which is better than what is expected from the luminosity increase ($\sim$ 40%) due to the MVA technique.

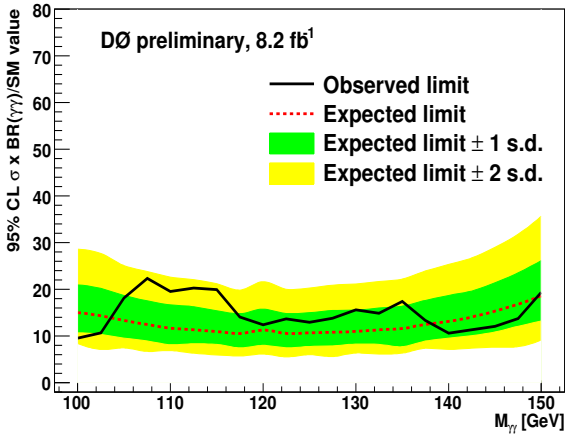

FIG. 5: 95% C.L. limits on the $\sigma \times BR$ relative to the SM prediction as a function of Higgs mass. The observed limit is shown as a solid black line while the expected limit under the background-only hypothesis is shown as a dashed red line. The green and yellow areas correspond to 1 and 2 standard deviations (s.d.) around the expected limit.

Acknowledgments

We thank the staff at Fermilab and collaborating institutions, and acknowledge support from the DOE and NSF (USA); CEA and CNRS/IN2P3 (France); FASI, Rosatom and RFBR (Russia); CAPES, CNPq, FAPERJ, FAPESP and FUNDUNESP (Brazil); DAE and DST (India); Colciencias (Colombia); CONACyT (Mexico); KRF and KOSEF (Korea); CONICET and UBACyT (Argentina); FOM (The Netherlands); STFC (United Kingdom); MSMT and GACR (Czech Republic); CRC Program, CFI, NSERC and WestGrid Project (Canada); BMBF and DFG (Germany); SFI (Ireland); The Swedish Research Council (Sweden); CAS and CNSF (China); and the Alexander von Humboldt Foundation.

[1] ALEPH, DELPHI, L3, and OPAL Collaborations, The LEP Working Group for Higgs Boson Searches, Phys. Lett. B **565**, 61 (2003).
[2] LEP Electroweak Working Group http://lepewwg.web.cern.ch/LEPEWWG/
[3] T. Aaltonen *et al.* (CDF Collaboration), Phys. Rev. Lett. **104**, 061803 (2010).
[4] V.M. Abazov *et al.* (DØ Collaboration), Phys. Rev. Lett. **104**, 061804 (2010).
[5] T. Aaltonen *et al.* (CDF and DØ Collaborations), Phys. Rev. Lett. **104**, 061802 (2010).
[6] T. Aaltonen *et al.* (CDF and DØ Collaborations), FERMILAB-CONF-10-257-E (2010).
[7] S. Mrenna and J. Wells, Phys. Rev. D **63**, 015006 (2000).
[8] DØ Collaboration, "Search for Light Higgs Boson in $\gamma\gamma$+X Final State with the DØ Detector at $\sqrt{s}$ = 1.96 TeV", DØ Note **5858-CONF** (2007).
[9] A. Hoecker *et al.*, TMVA 4 Toolkit for Multivariate Data Analysis with ROOT Users Guide, arXiv:physics/0703039 (2007).
[10] V. M. Abazov *et al.*, Nucl. Instrum. Meth. A **565**, 463 (2006).
[11] The polar angle θ and the azimuthal angle ϕ are defined with respect to the positive z axis, which is along the proton beam direction. Pseudorapidity is defined as $\eta = ln[tan(\theta/2)]$. Also, η_{det} and ϕ_{det} are the pseudorapidity and the azimuthal angle measured with respect to the center of the detector.
[12] T. Sjöstrand *et al.*, Comput. Phys. Commun. **135**, 238 (2001). We use PYTHIA version v6.323 with Tune A.
[13] H.L. Lai *et al.*, Phys. Rev. D **55**, 1280 (1997).
[14] R. Brun and F. Carminati, CERN Program Library Long Writeup W5013, 1993 (unpublished).
[15] The Tevatron New Phenomena and Higgs Working Group, "Cross Section and Branching Ratio Recommendations for Tevatron Higgs Searches", (2011).
[16] A. Djouadi, J. Kalinowski and M. Spira, Comput. Phys. Commun. **108**, 56 (1998).
[17] U. Aglietti *et al.*, arXiv:hep-ph/0610033 (2006).
[18] C. Peterson, T. Rognvaldsson and L. Lonnblad, "JETNET 3.0 A versatile Artificial Neural Nertwork Package", Lund University Preprint LU-TP 93-29. Version 3.5 is used here.
[19] R. Hamberg, W. L. van Neerven and T. Matsuura, Nucl. Phys. B **359**, 343 (1991) [Erratum-ibid. B **644**, 403 (2002)].

[20] Y. Liu, Ph.D. thesis, Fermilab [FERMILAB-THESIS-2004-37] (2004).
[21] T. Gleisberg *et al.* J. High Energy Phys. **02**, 007 (2009).
[22] T. Andeen *et al.*, FERMILAB-TM-2365 (2007).
[23] J. Pumplin *et al.*, JHEP **0207**, 012 (2002).
[24] W. Fisher, FERMILAB-TM-2386-E (2006).
[25] T. Junk, Nucl. Intrum. Meth. A **434**, 435 (1999); A. Read, CERN 2000-005 (30 May 2000).